

# Classification of rice planthoppers based on shape descriptors

eISSN 2051-3305

Received on 9th September 2019

Accepted on 30th September 2019

E-First on 25th November 2019

doi: 10.1049/joe.2019.1085

www.ietdl.org

Saihua Zhu<sup>1</sup>, Junyuan Zhang<sup>1</sup>, Xiangze Lin<sup>1</sup> ✉, Deying Liu<sup>1</sup>

<sup>1</sup>College of Engineering, Nanjing Agricultural University, Nanjing, People's Republic of China

✉ E-mail: xzlin@njau.edu.cn

**Abstract:** Here, classification of rice planthopper (RPH) based on shape descriptors was addressed to solve the low semantics problem of shape features in traditional RPH (mainly including the whiteback planthopper (*Sogatella furcifera* (Horváth)), the brown planthopper (*Nilaparvata lugens* (Stål)), and the small brown planthopper (*Laodelphax striatellus* (Fallén))) image classification research. Images of RPH were obtained from rice field by an automatic insect image acquisition device made by ourselves and insect images were divided into single images based on OTSU threshold segmentation algorithm. In terms of the images of RPH after segmentation, Fourier descriptors and Hu moments, which are from two aspects of contour curve and shape area, were extracted to describe shape features of RPH. Then, random forest (RF), an ensemble learning algorithm, was used as the classifier to distinguish RPH efficiently. The optimal number of trees and prediction variables of RF are chosen to be 150 and 4, respectively, by minimising the out-of-bag error. Experimental results show that classification accuracy of RPH based on shape descriptors reaches up to 93.93%. Therefore, it has been verified that the classification with the method presented here is accurate and semantic.

## 1 Introduction

Rice is one of the most important food sources of more than one-third of the world's population [1], and China is the largest rice-producing country in the world [2], where rice plays a leading role in agricultural production and food security. However, rice will be damaged by pests during various growth periods, which will bring serious negative impacts on the stable and high yield of rice [3]. Rice planthopper (RPH), mainly including the whiteback planthopper (WP) (*Sogatella furcifera* (Horváth)), the brown planthopper (*Nilaparvata lugens* (Stål)), and the small brown planthopper (*Laodelphax striatellus* (Fallén)), a migratory pest, is one of the main pests that affects rice growth. Then, a total of four to five million tons of rice grain are damaged by RPHs each year [4, 5]. Hence, it is essential to obtain pest population density of RPH in real time and develop relevant countermeasures in advance, which can keep the stable and high yield of rice. Currently, pest forecast of RPH still depends on manual counting, which will result in the inability to analyse data in time and prevent RPH effectively [6].

Hence, in order to realise the automation of the pest forecast of RPH, RPH image classification has become a hot research issue in recent years [7]. There exist numerous image recognition methods in RPH classification, such as [8–11]. [8] established the fisher discriminant function, which was used for the identification of RPH, based on the 2D spectrum data; In [9], rectangle regions of interest (ROIs) were gotten in HSV space and colour analysis was conducted, which showed that the results were useful to reduce executing time and loading and obtain image of RPHs. In [10], Fourier descriptors and Euclidean distance were applied to recognise RPH, and the average recognition rate is 92.15%; [11] proposed an automatic recognition method based on convolutional neural network. However, there are some disadvantages in the above RPH classification researches: after the morphological filtering operation of 'corrosion and expansion', the contours of RPH images will produce larger deformations, which will lead to lose its basic semantic information. Hence, to solve those problems, in this paper, the complete shape contour with Fourier descriptors and the complete shape region with Hu moments are combined to represent the shape descriptor, and WP images are distinguished from other insect images by the shape descriptors, which have a high classification accuracy. What is more, the

method presented in this paper can also be applied to recognise other RPH and other insect images.

The rest of the paper is organised as follows. RPH image acquisition and image preprocessing are given in Section 2. In Section 3, shape feature extraction of RPH is introduced. Experimental results are demonstrated and discussed in Section 4. Concluding remarks and future research are given in the last section.

## 2 Image acquisition and preprocessing of RPH

The outbreak period of RPH is from July to September each year in Jiangsu Province, East China. Therefore, in order to obtain enough test samples, we acquired the insect images in the rice fields from two areas in three times. One is Jiangpu Experimental Farm of Nanjing Agricultural University in Nanjing Pukou District (N32°01' E118°37') from August to October in 2015 and from June to October in 2016; the other is Baima National Agricultural Science and Technology Park in Nanjing Lishui District (N31°37' E119°10') from August to September in 2017. According to the characteristics of the phototaxis of RPH, the automatic insect image acquisition device, which is developed by our group ([12]), is used to obtain high-resolution images in sunny days with temperatures between 20 and 30 degrees Celsius and humidity between 6 and 8%, and Fig. 1 shows the RPH image acquisition device. In addition, the sampling time was from 18:00 to 20:00 every night. These captured pest images are 782\*576 pixels and saved as JPEG format. WP images and other non-RPH images are classified in this paper, which is as an example to explain the effectiveness and accuracy of the method presented in this paper. Certainly, this method can also be applied to classify the three types of RPH images and the other non-RPH images. For the sake of convenience, RPH refers to WP in the following sections. Image acquisition at experiment site and the original pest image are shown in Fig. 2.

After getting the original pest image, these pictures must be preprocessed at first. In order to facilitate shape features extraction, image segmentation and contour coordinate extraction are implemented in next subsections.

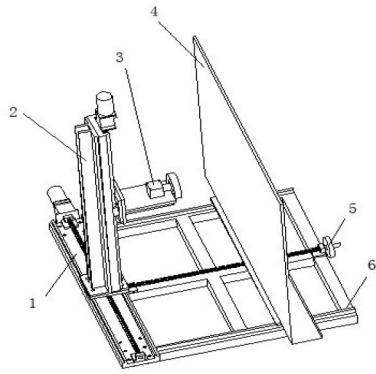


**Fig. 1** Structure of the image acquisition device: (1) X-direction adjustment device; (2) Z-direction adjustment device; (3) camera; (4) screen; (5) Y-direction adjustment device; (6) base



**Fig. 2** RPH image acquisition (a) Image acquisition at experiment site, (b) Original pest image

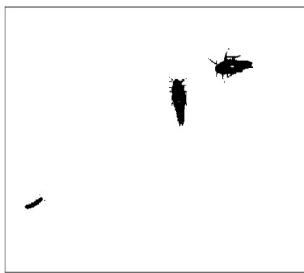


**Fig. 3** Original image processed by OTSU threshold segmentation

### 2.1 Image segmentation

In this section, original images in Fig. 2b, including 700 RPH images and 700 non-RPH images, are segmented into single insect images. It is well known that the OTSU threshold segmentation [13] is simple in computation and is not affected by image brightness and contrast. Hence, it is suitable for our experimental environment and can meet our needs. The image processed by OTSU threshold segmentation is shown in Fig. 3. After image segmentation, the original images are divided into single pest images, including 700 RPH images labelled as Class 1 and 700 non-RPH images (including leaf beetle (Chrysomelidae), rove beetle (Oxytelus batiuculus), leafhopper (Cicadellidae), lygaeid bug (Lygaeidae), ant (Pheidole megacephala (Fabricius) etc.) labelled as Class 0. All single pest images are 300\*300 pixels and saved as JPEG format. Fig. 4 shows some single pest images after segmentation, and RPH (A) and RPH (B) are WPs; non-RPH (A) is leaf beetle and non-RPH (B) is rove beetle.

### 2.2 Contour coordinates extraction

In this subsection, contour coordinates of insects are extracted and then the dimension of these insect contour coordinate dataset is reduced.

For the 1400 single pest images after the above-mentioned segmentation, contour coordinates are extracted one by one. The process of contour coordinates extraction is as follows

(i) Convert the single pest images to binary images and assume that the first point in the upper left corner of the image is the coordinate

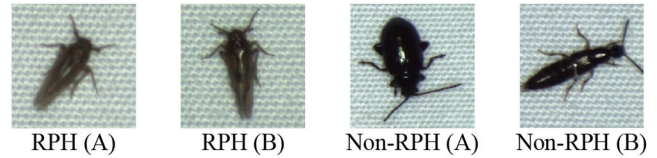


**Fig. 4** Different pest images after segmentation

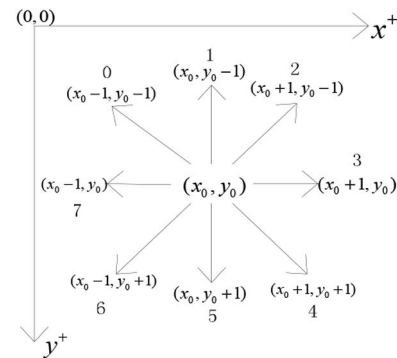


**Fig. 5** Order of inspection

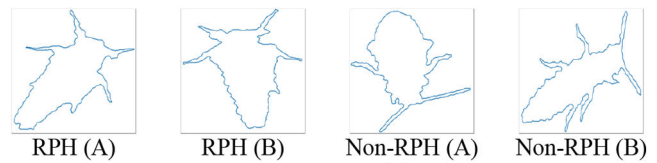


**Fig. 6** Contours of different pests

origin (0, 0). Check all image pixels and mark those points, where the left and right values are not equal, as the contour points [14] and let the points with a value equal to 1 be the contour coordinates. Thus, the contour coordinate dataset is  $\{F_n = (x_i, y_i), i = 0, 1, 2, \dots, N - 1\}$ .

(ii) Select a coordinate as the starting point of the contour curve randomly, denoted by  $(x_0, y_0)$ , then delete this coordinate from the contour coordinate dataset. Let the upper left coordinate  $(x_0 - 1, y_0 - 1)$  of the starting point be denoted as 0, and the other adjacent coordinates of the starting point are also coded by using a numbering scheme, as in Fig. 5. Then, check the contour coordinate dataset in the order of 0 to 7 and set the coordinate, which first appears in the above order, as the next contour coordinate  $(x_i, y_i)$ . In addition, delete this coordinate from coordinate dataset.

(iii) Let the coordinate  $(x_i, y_i)$  be a new starting point and repeat Step 2 until all coordinates are sequentially connected [15].

According to the above method, contours of the pests in Fig. 3 are shown in Fig. 6.

The comparison between the contours extracted by the method in [12] (denoted as Contour (I)) and the contours extracted by the method proposed in this paper (denoted as Contour (II)) are shown in Fig. 7. From comparison results, it is not difficult to see that the contours of the pests extracted by the method presented in this paper have more details, more semantics and can express more shape information than that in [12].

For the coordinate dataset is very huge, it will spend lots of time extracting the shape features. In order to increase the efficiency of computation, dimension of the coordinate dataset should be reduced [16]. Under the premise of maintaining the intact shape, we only take one-third of the original coordinate dataset for subsequent operations. Then, the specific steps are shown in Procedure 1 (see Fig. 8).

Contours of the pests after the dimensionality reduction algorithm and the original contours are shown in Fig. 9. From Fig. 9, it can be seen that, compared with the original contour, the shape of the contour is almost invariable after the dimensionality reduction, and only the inessential details are ignored.

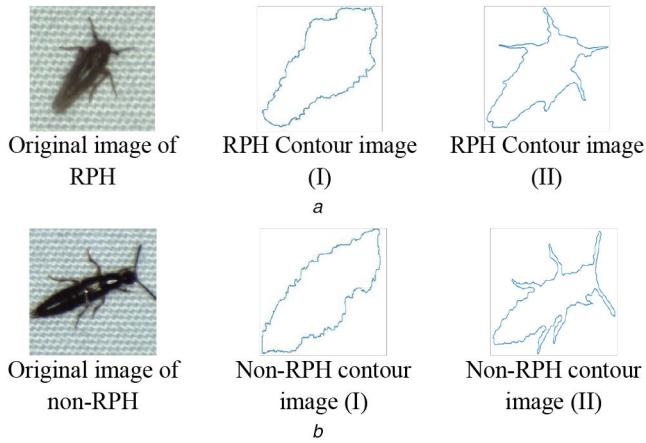


**Fig. 7** Contour extraction of different insects  
(a) RPH and its contour image, (b) Non-RPH and its contour image

```

procedure Dimensionality_Reduction(dataset)
  ▷ dataset[i]={(xi,yi) | i = 0,1,2,...,N-1}
  if (N%3==1)
    delete dataset[N-1]
  else if (N%3==2)
    delete dataset[N-1]
    delete dataset[N-2]
  for(i=0,i<=N-1,i=i+3)
    xi ← (xi + xi+1 + xi+2) / 3
    yi ← (yi + yi+1 + yi+2) / 3
  return dataset

```

**Fig. 8** Procedure 1 – dimensionality reduction algorithm

### 3 Shape feature extraction of RPH

In order to describe the shape features of RPH better, the shape features from two aspects, contour curve and shape region, are extracted.

#### 3.1 Fourier descriptor

Fourier descriptors [17, 18] are obtained by applying the discrete Fourier transform over a shape signature and are contour-based shape descriptors. In this paper, Fourier descriptor is used to depict contour curve features of insects.

According to [10], first 15 coefficients of discrete Fourier transform are chosen as Fourier descriptors. To perform a discrete Fourier transform operation on the dataset, the first 15 coefficients are obtained and the normalisation Fourier descriptors are denoted as {FD(1), FD(2), ..., FD(13)}. The normalised Fourier descriptors extracted from the contour curve obtained by the method in this paper (denoted as Method I) and the method in [12] (denoted as Method II) are shown in Table 1.

From Table 1, in the case of Method I, it is not difficult to see that the Fourier descriptors of RPH (RPH (A) and RPH (B)) have little difference, while different categories of pests have greatly different Fourier descriptors, for example FD<sub>1</sub>, FD<sub>2</sub> of RPH (A) are similar to RPH (B)'s; FD<sub>1</sub>, FD<sub>2</sub> of RPH are quite different from non-RPH's. Therefore, RPH and non-RPH can be well distinguished by Method I proposed in this paper. However, by virtue of the Method II, the Fourier descriptors of RPH (A) and RPH (B) are dissimilar and confused with non-RPH, for example FD<sub>1</sub>, FD<sub>2</sub> of RPH (A) are similar to non-RPH (A) and non-RPH (B)'s, which easily lead to misclassification. Hence, for the efficient classification of RPH and non-RPH, Method I is better than Method II, and based on these Fourier descriptors extracted

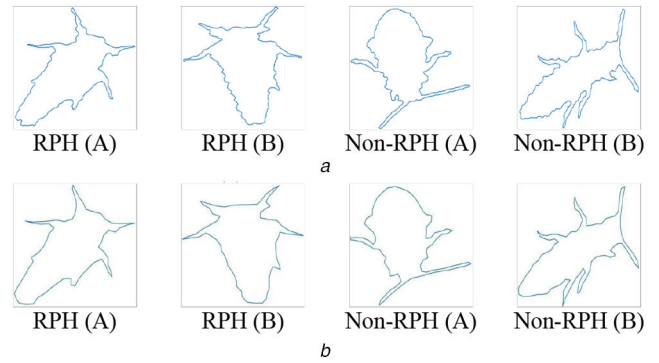


**Fig. 9** Results of contour dimensionality reduction  
(a) The original RPH contours, (b) The RPH contours after the dimensionality reduction

from complete shape of RPH which is used in this paper, namely Method I, RPH and non-RPH can be effectively classified.

#### 3.2 Hu moment

Hu moments [19, 20] are region-based shape descriptors and invariant to translation, scale change, mirroring, and rotation, which can describe the shape information effectively. In this subsection, Hu moment is utilised to represent shape region features of insects [21].

According to [18], Hu moments extracted from the shape region obtained by the method in this paper (denoted as Method I) and the method in [12] (denoted as Method II) are shown in Table 2.

From Table 2, under the condition of Method I, it can be seen that Hu moments of RPH, see RPH (A) and RPH (B), are similar, including the same symbol and the same order of magnitude. In addition, Hu moments of different categories of pests have a great difference, so RPH and non-RPH can be well distinguished by Hu moment in Method I. When Method II is applied, the differences between Hu moments of RPH (A) and RPH (B) are very large, so Hu moment in Method II cannot be used as effective classification feature. Compared with Method II, Method I has obvious advantages in RPH image classification. Thus, Hu moments extracted from complete shape of RPH, that is Method I, can be used as shape descriptors and RPH and non-RPH can be well classified.

### 4 Random forest classification

Random forest (RF) is one of the ensemble learning algorithms, which are more accurate and robust to noise than single classifiers [22, 23]. What is more, RF runs on large dataset and can estimate missing data and maintains accuracy when a large proportion of the data are missing, efficiently. Thus, taking its ability to process data and robustness into consideration, RF is applied to classify the RPH and non-RPH images.

#### 4.1 Selection of classifier optimal parameters

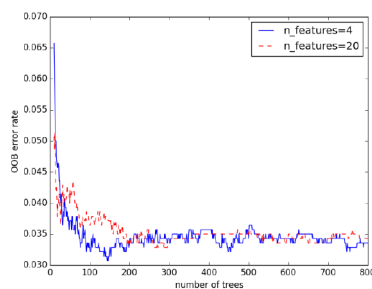
Compared with classification trees, RF needs to consider the number of trees ( $k$ ) except the number of prediction variables ( $N$ , the sum of number of Fourier descriptor and number of Hu moment, i.e.  $N = 13 + 7 = 20$  in this paper), so the complexity of this classification is  $O(k(Nn \log n))$ , where  $n$  is the amount of the dataset [24]. According to [25, 26], the number of trees is generally 100 for most classification problems, and for a given dataset has fixed number of feature  $N$ , the number of prediction variables can be taken as  $\log_2^N$ ,  $\sqrt{N}$ , and  $N$ . In this paper,  $N$  is equal to 20 and  $\log_2^N = \sqrt{N} = 4$ . When deciding the number of trees, although larger values of  $k$  resulted in more stable classifications and variable importance measures, the calculation cost must also be considered. Therefore, in order to improve the operating efficiency of the classifier while obtaining the best classification effect, out-of-bag (OOB, the samples which are not present in the calibration subset are included as part of another subset) error is used to find

**Table 1** Normalised Fourier descriptors for different pests

Fourier descriptors	RPH (A)		RPH (B)		Non-RPH (A)		Non-RPH (B)	
	Method I	Method II	Method I	Method II	Method I	Method II	Method I	Method II
FD(1)	0.562	9.421	0.588	2.318	2.821	10.88	0.064	9.344
FD(2)	0.350	1.047	0.475	0.693	2.439	1.194	0.048	0.248
FD(3)	0.696	0.272	0.325	0.128	1.578	0.553	0.274	0.763
FD(4)	0.631	0.537	0.487	0.210	2.014	0.448	0.214	0.391
FD(5)	0.184	0.877	0.202	0.207	1.041	0.376	0.423	0.211
FD(6)	0.301	0.139	0.232	0.170	0.881	0.124	0.109	0.322
FD(7)	0.074	0.410	0.026	0.193	0.648	0.954	0.070	0.068
FD(8)	0.069	0.643	0.117	0.155	0.571	1.342	0.165	0.106
FD(9)	0.172	0.246	0.038	0.017	0.516	0.926	0.113	0.148
FD(10)	0.026	0.297	0.027	0.027	0.324	0.473	0.051	0.285
FD(11)	0.012	0.295	0.027	0.102	0.215	0.275	0.037	0.055
FD(12)	0.038	0.420	0.032	0.072	0.430	0.125	0.076	0.235
FD(13)	0.052	0.223	0.061	0.053	0.130	0.102	0.010	0.034

**Table 2** Hu moment for different pests

Hu moment		RPH (A)	RPH (B)	Non-RPH (A)	Non-RPH (B)
$\phi_1$	Method I	$2.525 \times 10^{-01}$	$2.626 \times 10^{-01}$	$2.411 \times 10^{-01}$	$3.677 \times 10^{-01}$
	Method II	$1.970 \times 10^{-01}$	$2.028 \times 10^{-01}$	$1.760 \times 10^{-01}$	$1.927 \times 10^{-01}$
$\phi_2$	Method I	$2.806 \times 10^{-03}$	$3.162 \times 10^{-02}$	$6.125 \times 10^{-03}$	$8.999 \times 10^{-02}$
	Method II	$7.105 \times 10^{-06}$	$1.072 \times 10^{-05}$	$3.118 \times 10^{-08}$	$2.373 \times 10^{-05}$
$\phi_3$	Method I	$1.964 \times 10^{-03}$	$3.213 \times 10^{-03}$	$3.561 \times 10^{-04}$	$2.266 \times 10^{-04}$
	Method II	$4.805 \times 10^{-07}$	$3.047 \times 10^{-07}$	$1.637 \times 10^{-10}$	$9.297 \times 10^{-07}$
$\phi_4$	Method I	$2.390 \times 10^{-04}$	$5.027 \times 10^{-04}$	$4.276 \times 10^{-05}$	$5.694 \times 10^{-04}$
	Method II	$3.660 \times 10^{-06}$	$5.351 \times 10^{-07}$	$4.417 \times 10^{-08}$	$3.580 \times 10^{-06}$
$\phi_5$	Method I	$1.431 \times 10^{-07}$	$6.322 \times 10^{-07}$	$-1.774 \times 10^{-09}$	$1.005 \times 10^{-07}$
	Method II	$-4.071 \times 10^{-12}$	$-9.285 \times 10^{-14}$	$-4.033 \times 10^{-17}$	$-6.434 \times 10^{-12}$
$\phi_6$	Method I	$3.305 \times 10^{-05}$	$8.859 \times 10^{-05}$	$-3.332 \times 10^{-06}$	$1.600 \times 10^{-04}$
	Method II	$-8.743 \times 10^{-09}$	$-1.018 \times 10^{-09}$	$-3.715 \times 10^{-12}$	$-1.733 \times 10^{-08}$
$\phi_7$	Method I	$-7.963 \times 10^{-08}$	$-9.317 \times 10^{-08}$	$4.961 \times 10^{-09}$	$1.781 \times 10^{-07}$
	Method II	$2.656 \times 10^{-12}$	$1.954 \times 10^{-13}$	$-1.112 \times 10^{-16}$	$1.100 \times 10^{-12}$

**Fig. 10** Effect of number of trees and prediction variables on OOB error

the optimal number of trees [27]. Fig. 10 shows the OOB error depending on the number of trees where the number of prediction variables is chosen as 4 or 20 according to [25, 26].

From Fig. 10, it can be seen when the number of trees gradually increases from 0, the OOB error decreases rapidly. Then when the number of trees exceeds 60, the OOB error is lower than 4.3%, which means that RF can be effectively classify RPH under the condition that the prediction variables is 4 or 20. When the number of trees and prediction variables are 150 and 4, respectively, the OOB error has a minimum value of 3.1%. Meanwhile, the OOB error converges 3.4% regardless of the value of the feature number and the addition of more trees neither increases nor decreases the OOB error. Thus, in order to gain the optimal classification accuracy and the best operation efficiency, the number of trees and prediction variables are chosen as 150 and 4, respectively.

#### 4.2 Experimental results

In this RF classification experiment, the experimental samples consist of 700 RPH images and 700 non-RPH images, a total of 1400 pieces. The 1400 images are randomly divided into five copies and each copy has 280 images, which facilitate cross-validation. The feature parameters consist of 13 normalised Fourier descriptors and 7 Hu moments (20 in total), i.e. {FD(1), FD(2), ..., FD(13),  $\phi_1, \phi_2, \dots, \phi_7$ }. The optimal parameters of RF for this paper are first verified. When the number of trees are 100 [25, 26] and 150 (according to the optimal method in this paper) and the number of prediction variables are 4 and 20, respectively, the performance of RF are shown in Table 3.

From Table 3, it is shown that the optimal numbers of trees and prediction variables are 150 and 4, and the accuracy and the F1 score are 93.93% and 0.94, which are the best among these accuracy and F1 score. In addition, when the number of trees is taken as 150, the model evaluation indexes all beyond 90% and are significantly better than those whose number of trees is 100, which proves that larger values of tree number resulted in more stable classifications. In general, the F1 score are all above 0.8, reflecting the strong stability and robustness of this classifier. Therefore, RF can be used to recognise RPH images efficiently.

Then, the method proposed in this paper and the method proposed in [12] are tested, respectively, when the number of trees and prediction variables are 150 and 4, respectively, in RF. The comparison results are shown in Table 4.

The test results shown in Table 4 demonstrate that, on the one hand, the accuracy, precision and recall of the method proposed in this paper are all over 90%, which are fully superior to the method

**Table 3** Performance of RF under different conditions

Model evaluation index	The number of trees and the number of prediction variables			
	150 and 4	150 and 20	100 and 4	100 and 20
accuracy, %	93.93	90.71	84.64	89.64
precision, %	92.67	90.00	70.92	87.14
recall, %	95.76	93.30	98.04	91.73
F1 score	0.94	0.91	0.82	0.89

**Table 4** Test accuracy under different methods

Model evaluation index	Method in this paper	Method in [12]
accuracy, %	93.93	67.14
precision, %	92.67	68.15
recall, %	95.76	65.71
F1 score	0.94	0.67

proposed in [12]. On the other hand, the model evaluation indexes in [12] are just between 60 and 70%, which means that corroded shapes are not able to be used as valid feature of RPH classification. The accuracy in this paper is 93.93%, while the accuracy in [12] is only 90.91%, so the method proposed in this paper meets the actual requirement when the RPH images are classified by the method based on shape descriptors.

## 5 Conclusion

In this study, a RPH recognition method based on shape descriptors has been developed. Fourier descriptor and Hu moment have been used to represent the complete shape information of RPH, which are from two aspects of the contour curve and the shape region. Moreover, RF has been applied to recognise RPH images and the accuracy of classification reaches up to 93.93%, which means that the RPH image classification method presented in this paper can be applied to the automatic measurement of rice pests and diseases and reduce labour intensity of pest forecast. In a future study, colour, texture, and other features, combined with shape features, will be utilised as feature parameters to improve the classification accuracy.

## 6 Acknowledgments

This work was supported by the Natural Science Foundation of China (Grant No. 61773216), Natural Science Foundation of Jiangsu Province of China (Grant No. BK20171386).

## 7 References

- [1] Lakshminarayana, R.V., Satyavathi, V.V., Siddiq, E.A., *et al.*: 'Review of methods for the detection and quantification of adulteration of rice: Basmati as a case study', *J. Food Sci. Technol.*, 2015, **52**, (6), pp. 3187–3202
- [2] Huang, S.W., Wang, L., Liu, L.M., *et al.*: 'Nonchemical pest control in China rice: a review', *Agronomy Sust. Dev.*, 2014, **34**, (2), pp. 275–291
- [3] Sumitra, A., Mukesh, S., Srivastava, D.S., *et al.*: 'Rice pest management with reduced risk pesticides in India', *Environ. Monit. Assess.*, 2019, **191**, p. 241
- [4] Anuwat, L., Jarongsak, P., Ammorn, I.: 'Effectiveness of nano plant essential oils against brown planthopper, *nilaparvata lugens* (stål)', *Int. J. Agric. Technol.*, 2017, **13**, (7.2), pp. 1537–1546
- [5] Masaya, M., Sachiyo, S., Morimura, A.O., *et al.*: 'Insecticide susceptibilities of the two rice planthoppers *nilaparvata lugens* and *sogatella furcifera* in East Asia, the Red River Delta, and the Mekong Delta', *Pest Manag. Sci.*, 2018, **74**, pp. 456–464
- [6] Li, X.Z., Zou, Y., Yang, Y.H., *et al.*: 'Meteorological driven factors of population growth in brown planthopper, *nilaparvata lugens* stål (Hemiptera: delphacidae), in rice paddies', *Entomol. Res.*, 2017, **47**, pp. 309–317
- [7] Deng, L.M., Wang, Y.J., Han, Z.Z., *et al.*: 'Research on insect pest image detection and recognition based on bio-inspired methods', *Biosystems Eng.*, 2018, **169**, pp. 139–148
- [8] Yu, M.H., Wang, J.L., Kang, R., *et al.*: 'Automatic identification of asian rice plant-hopper based on image processing', *Appl. Eng. Agric.*, 2017, **33**, (5), pp. 591–602
- [9] Tsai, T.H., Lee, T.Y., Chen, P.H., *et al.*: 'The ROI of rice planthopper by image processing'. IEEE Int. Conf. on Applied System Innovation, Sapporo, Japan, May 2017, pp. 126–129
- [10] Zhao, S.Q., Liu, D.Y., Ding, W.M., *et al.*: 'Influence of outline points on the recognition accuracy of Fourier descriptors', *Trans. Chinese Soc. Agric. Mach.*, 2014, **45**, (9), pp. 305–310
- [11] Liu, D.Y., Wang, J.L., Lin, X.Z., *et al.*: 'Automatic identification method for *sogatella furcifera* based on convolutional neural network', *Trans. Chinese Soc. Agric. Mach.*, 2018, **49**, (5), pp. 51–56
- [12] Xie, T.S., Liu, D.Y., Chen, J., *et al.*: 'Automatic identification of *sogatella furcifera*', *J. Nanjing Agric. Univ.*, 2016, **39**, (3), pp. 519–526
- [13] Otsu, A.: 'Threshold selection method from gray-level histogram', *IEEE Trans. SMC29*, 1979, **9**, (3), pp. 62–66
- [14] Freeman, H.: 'On the encoding of arbitrary geometric configurations', *IEEE Trans. Electron. Comput. EC*, 1961, **10**, pp. 260–268
- [15] Pawel, K., Adam, K., Witold, P., *et al.*: 'An application of chain code-based local descriptor and its extension to face recognition', *Pattern Recognit.*, 2017, **65**, pp. 26–34
- [16] Vargas, J., Sorzana, C.O.S., Antonio, Q.J., *et al.*: 'Fringe pattern denoising by image dimensionality reduction', *Opt. Lasers Eng.*, 2013, **51**, pp. 921–928
- [17] Zahn, C.T., Roskies, R.Z.: 'Fourier descriptors for plane closed curves', *IEEE Trans. Comput.*, 1992, **21**, (3), pp. 269–281
- [18] Gonzales, R.C., Woods, R.E.: 'Digital image processing' (Person Education, London, UK, 2011, 3rd edn.)
- [19] Wong, Y.R.: 'Scene matching with invariant moments', *Comput. Graph. Image Process.*, 1978, **8**, (1), pp. 16–24
- [20] Flusser, J., Suk, T.: 'Pattern recognition by affine moment invariant', *Pattern Recognit.*, 1993, **26**, (1), pp. 167–174
- [21] Rhouma, M.B.H., Joviša, Z., Younis, M.C.: 'Moment invariants for multi-component shapes with applications to leaf classification', *Comput. Electron. Agric.*, 2017, **142**, pp. 326–337
- [22] Breiman, L.: 'Bagging predictors', *Mach. Learn.*, 1996, **24**, (2), pp. 123–140
- [23] Dieterich, T.G.: 'An experimental comparison of three methods for constructing ensembles of decision trees: bagging, boosting, and randomization', *Mach. Learn.*, 2000, **40**, (2), pp. 139–157
- [24] Xu, H., Wang, W.J., Ren, L.F.: 'A method for monotonic classification based on decision forest', *J. Comput. Res. Dev.*, 2017, **54**, (7), pp. 1477–1487
- [25] Rodriguez-Galiano, V.F., Ghimire, B., Rogan, J., *et al.*: 'An assessment of the effectiveness of a random forest classifier for land-cover classification', *ISPRS J. Photogramm. Remote Sens.*, 2012, **67**, pp. 93–104
- [26] Liu, M., Lang, R.L., Cao, Y.B.: 'Number of trees in random forest', *Comput. Eng. Applic.*, 2015, **51**, (5), pp. 126–131
- [27] Aijen, J., Camille, M., Margrit, B., *et al.*: 'Comparing random forest approaches to segmenting and classifying gestures', *Image Vis. Comput.*, 2017, **58**, pp. 86–95